Hindawi
International Transactions on Electrical Energy Systems
Volume 2023, Article ID 6902796, 15 pages
https://doi.org/10.1155/2023/6902796

Research Article

Dynamic Performance Improvement of a Single-Phase VSI with Digital Implementation of an On-Line Optimal Trajectory Control Algorithm

Shah Zaman, Yan Zhang, Jinjun Liu, Danni Yang, and Zhenchao Li

Electrical engineering, Xi'an Jiaotong University China, Xi'an, Shaanxi, China

Correspondence should be addressed to Jinjun Liu; jjliu@mail.xjtu.edu.cn

Received 1 December 2022; Revised 23 January 2023; Accepted 5 April 2023; Published 20 April 2023

Academic Editor: Anjanee Kumar Mishra

A single-phase voltage source inverter (VSI) still suffers from a long settling time and significant voltage overshoot/undershoot under the abrupt step-change of load current. This article analyzes the comprehensive large-signal dynamic process and limitation of the linear controller during step change in load current. The combination of linear and nonlinear control is presented which is a realistic, simple, and low-cost technique for enhancing the dynamic response of the single-phase VSI. A nonlinear controller based on the simplified capacitor charge balance algorithm is employed to drive the inductor current and capacitor voltage to attain the target value by precisely following the projected optimal trajectory during the transient process in a brief period. A linear PI controller is utilized during the steady-state operations such as input voltage variations, temperature drifts, and component ageing. The complete mathematical derivation as well as a design method is presented to guide the practical hardware implementation for the given main circuit parameters and identified load step change. Even though accurate time instants can be obtained using off-line numerical calculations, reasonable simplifications are provided for real-time practical engineering applications in DSP. Finally, simulation and experimental verifications prove that the single-phase VSI achieves a substantial settling time decrease and reduced voltage oscillations.

1. Introduction

Single-phase alternating current power supplies are commonly used in applications such as active power filters, solar power generating systems, and laboratory testing, including power equipment research and development and electrical manufacturing. When delivering a load that fluctuates too quickly between many steady-state locations, most single-phase VSIs still have a lengthy settling period and severe voltage overshoot/undershoot. Under a 10% to 80% load step change, the usual transient recovery time is larger than 2 ms, which does not match the high-precision test requirement. As a result, significant research efforts have been directed into improving the dynamic performance of high-precision single-phase AC power sources delivering the impact load in recent years [1, 2].

Traditional linear control techniques, such as PI and PR [3–7], are best suited for situations with gradual load changes. However, in applications that need quick and precise current monitoring, the dynamic response of these kinds of current controllers is often poor. A nonlinear control technique is intensively investigated to increase the dynamic performance because it responds too rapidly to transients. Nevertheless, the majority of them may lead to undesirable performance, such as nonzero steady-state error and varying switching frequency. For example, the critical parameters of deadbeat [8] are developed considering the particular information of load conditions. It is challenging to calculate these characteristics when there are large fluctuations in the load. The hysteresis control [9–11] provides virtually instantaneous reference tracking and is impervious to instability problems but at the expense of variable switching frequency and higher control complexity. Dead

time affects current-tracking precision, switching frequency, and duty cycle range for parabolic current-controlled VSIs [12, 13]. The advantages of sliding mode control (SMC) [14–16] include rapid dynamic reaction, rejection of external disturbances, and insensitivity to parameter fluctuations. However, it is difficult to obtain a suitable sliding surface. In addition, boundary control (BC) [17–19] and H-infinity [20] are options for enhancing the dynamic performance. BC and H-infinity are effective but hard to implement.

Combining linear and nonlinear control techniques (PI + non-linear) is used to fully use their benefits, using a nonlinear controller during the transient and a linear controller in the steady state to speed up the transient behaviour and preserve strong steady-state performance. This nonlinear control approach forecasts the best trajectory for single-phase inverters under varying loads. It determines the appropriate switching sequences to force the converter to move from one steady state to another to regain lost charge. This can be performed by fixing the duty cycle high (for a step-up change) and low (for a step-down change) for a specified interval and followed by low (for a step-up change) and high (for a step-down change) for the additional interval. Thus, the controller enhances the dynamic response (reduced settling time and minimal output voltage undershoot/overshoot) undergoing fast load changes.

In the literature [21, 22], a straightforward design strategy for traditional DC-DC converters was given. The capacitor charge balance control (CBC) method is used to calculate the on- and off-state time intervals of power devices [21, 23–31]. It has been shown that the quickest transient response may be attained in a single switching period. And its fundamental concept is to estimate the ideal dynamic trajectory and establish the precise switching sequence of the power device to drive the converter from one steady-state to another in response to rapid load shift. Under conditions of rapid load changes, the single-phase VSI's output voltage and inductor current fluctuate frequently. As a result, enhanced CBC is offered since the traditional CBC strategy cannot be utilized to the single-phase VSI to boost dynamic response. This article first analyzes the comprehensive large signal dynamic model and transient response limitation of the single-phase VSI in Section 2. Section 3 proposes an online trajectory approach for properly monitoring the projected ideal trajectory during the transient phase, therefore causing the inductor current to achieve the desired value. The method for designing system control and the precise mathematical derivation are both provided in Section 4. Section 5 provides examples of both simulation and experimental validation. The last portion is the conclusion.

2. Single-phase VSI Load Step Challenges

The basic circuit of a single-phase full-bridge VSI is seen in Figure 1, and it supplies the pure resistive load R_{L1} with the help of an LC filter. The additional switch S_d simulates abrupt load change by connecting or disconnecting R_{L2}.

As an example of fundamental analysis, a single-phase VSI with the bipolar pulse width modulation (PWM) approach is chosen and modelled for the research. Two pairs of

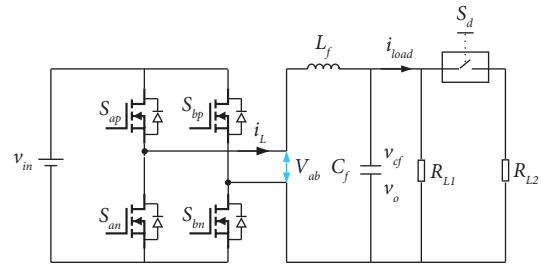

Figure 1: The single-phase full-bridge VSI.

switches (S_{ap} and S_{bn}) and (S_{bp} and S_{an}) work in complementary states. According to the switching state, there are two equivalent circuits, as shown in Figure 2. When $S_{ap} = S_{bn} = \text{ON}$ and $S_{bp} = S_{an} = \text{OFF}$, the energy flows through S_{ap} and S_{bn} to supply R_{L1} via the LC filter as demonstrated in Figure 2(a). When $S_{bp} = S_{an} = \text{ON}$ and $S_{ap} = S_{bn} = \text{OFF}$, the power source energy flows through S_{bp} and S_{an} to provide R_{L1} via the LC filter, as shown in Figure 2(b).

Figure 3 depicts the transient response waveform of the single-phase VSI with a linear controller when the load current is abruptly increased or decreased. As seen by the red waveform, i_{load} quickly changes from its starting value $I_{o1}\sin(\theta)$ to $I_{o2}\sin(\theta)$ when S_d is turned on at θ_0. However, the inductor current i_L cannot fluctuate too rapidly to match the required load current. Cf thus compensates the transitory current. As for the positive load current change shown in Figure 3(a), the error, sampling voltage feedback signal $v_o^{'}$compared with v_{ref}, is amplified to increase i_{ref}. i_L is slowly growing. Until θ_1 when i_L equals i_{load}, i_{load} is still higher than i_L, and v_o continues to decline.

After θ_1, i_L keeps growing and is higher than i_{load} $C_f$when it begins recharging. $v_o$rises and exceeds the reference value. At θ_2, i_L declines and equals to i_{load} again. C_f begins discharging, and $v_o$tends to be close to the reference value. Until θ_3, both i_L and v_{Cf} are close to $I_{o2}\sin(\theta)$ and v_{ref} and the new steady-state single-phase VSI is reached.

Most of the time, this fluctuation process continues for a long time until it recovers from one steady-state to another steady-state after a sudden change in load. A good tradeoff between the voltage/current overshoot/undershoot and dynamic regulation time should be considered for the optimal parameter design of the linear controller. Furthermore, the dynamic regulation time is increased too much due to the sudden load step-change magnitude under the relatively low switching frequency.

3. On-Line Trajectory Control for the Single-Phase VSI

As seen in Section 2, the single-phase VSI with a standard controller still exhibits a long settling period, and substantial voltage overshoots and undershoots in response to rapid changes in load current. To overcome the challenge, an online optimal trajectory control as an improved nonlinear predictive digital control method is proposed to improve the dynamic response as the problem terminator [32]. The fundamental concept is identifying optimal trajectory by

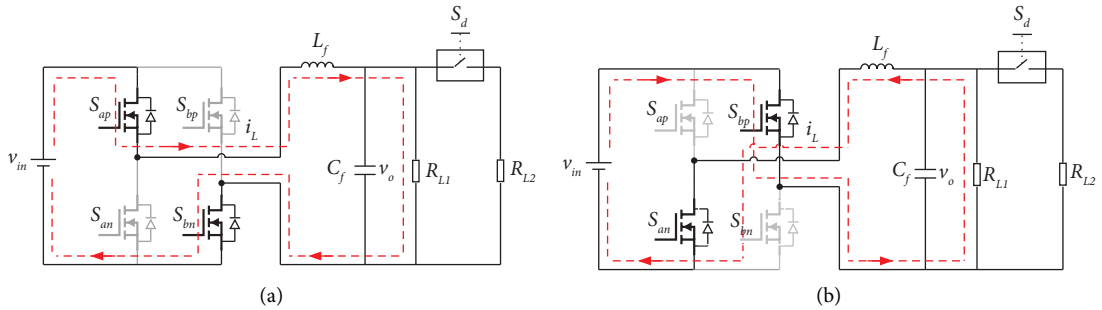

FIGURE 2: The equivalent circuit of the full-bridge single-phase VSI. (a) $S_{ap} = S_{bn} = \text{ON}$ and $S_{bp} = S_{an} = \text{OFF}$. (b) $S_{an} = S_{bp} = \text{ON}$ and $S_{ap} = S_{bn} = \text{OFF}$.

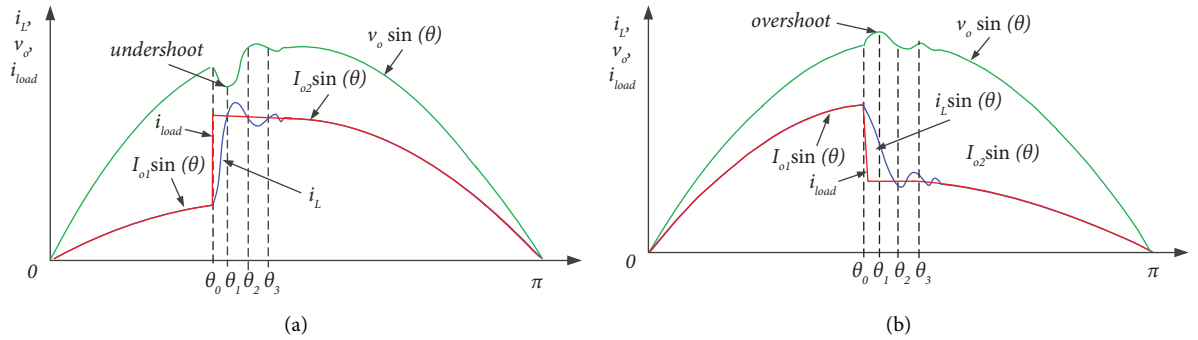

FIGURE 3: Transient response of the single-phase VSI with the linear controller in response to load current. (a) Positive step change. (b) Negative step change.

examining the large signal dynamic process when the load changes abruptly. In response to load variation, the projected ideal waveforms of capacitor voltage and inductor current from the initial steady state to the final steady-state are shown in Figure 4.

The suggested controller incorporates two distinct controls: a linear controller for steady-state operation and a nonlinear controller for transient situations. The capacitor current will provide the necessary current since the inductor current does not vary immediately in response to load current variations. The capacitor charge balance theory states that the charge supplied to the capacitor S_1 (discharge) at the end of the transient cycle must equal the charge withdrawn from the capacitor S_2 (charge), as shown in Figure 4(a). As S_1 has been reduced, the recharging part S_2 has also been reduced. The time required to charge S2 must be reduced in order to decrease the settling time. According to Figure 4(a), the time necessary to recharge the capacitor t_{ch} may be shortened by increasing the height h of the S_2 triangle (defined by θ_0–θ_2); this is achieved by fixing the duty ratio to 100% for θ_0–θ_2 and 0% for θ_2-θ_3.

The recommended controller is intended to do the following:

(i) Determine whether there is an abrupt load shift.

(ii) Fix the duty ratio to 100% (θ_0–θ_2) and 0% (θ_2-θ_3) for a step-up change in a positive half cycle; for a step-down change, fix the duty ratio to 0% (θ_0–θ_2) and 100% (θ_2-θ_3) in a negative half cycle.

(iii) Fix the duty ratio to 0% (θ_0–θ_2) and 100% (θ_2-θ_3) for a step-down change in a positive half cycle; for a step-up change, set the duty ratio to 100% (θ_0–θ_2) and 0% (θ_2-θ_3) in a negative half cycle.

(iv) Switch back to the linear controller once again.

Figure 4 shows the projected ideal waveforms of i_L and v_{Cf} throughout the transient process with positive and negative load current fluctuations. The trainset regulation process is divided into three-time intervals for detailed analysis.

The red waveform depicts the instantaneous transition in i_{load} from $I_{o1}\sin(\theta)$ to $I_{o2}\sin(\theta)$ when Sd is activated at θ_0. i_L cannot vary rapidly to maintain the required load current at θ_0. To speed up the transient, once the positive step change of i_{load} is detected, as shown in Figure 4(a), $S_{ap} = S_{bn} = \text{ON}$ and $S_{an} = S_{bp} = \text{OFF}$ are set instantly to rise i_L. Until θ_1, when $i_L = I_{o2}\sin(\theta_1)$, v_{Cf} declines to deliver the necessary load current. After θ_1, i_L rises higher than $I_{o2}\sin(\theta)$, and v_o begins to rise. The inductor current rising slope during θ_1 and θ_2 may be described using the equivalent circuit depicted in Figure 2(a) as follows:

$$k_1 = \frac{v_{in} - v_o \sin(\theta)}{2L\pi f_{line}}. \tag{1}$$

At θ_2, $S_{an} = S_{bp} = \text{ON}$, $S_{ap} = S_{bn} = \text{OFF}$, and i_L begin to decline as v_{Cf} grows. At θ_3, i_L is close to the load current, and v_o is back to the reference voltage. Both i_L and v_{Cf} enter the quasi-steady state. The inductor current falling slope

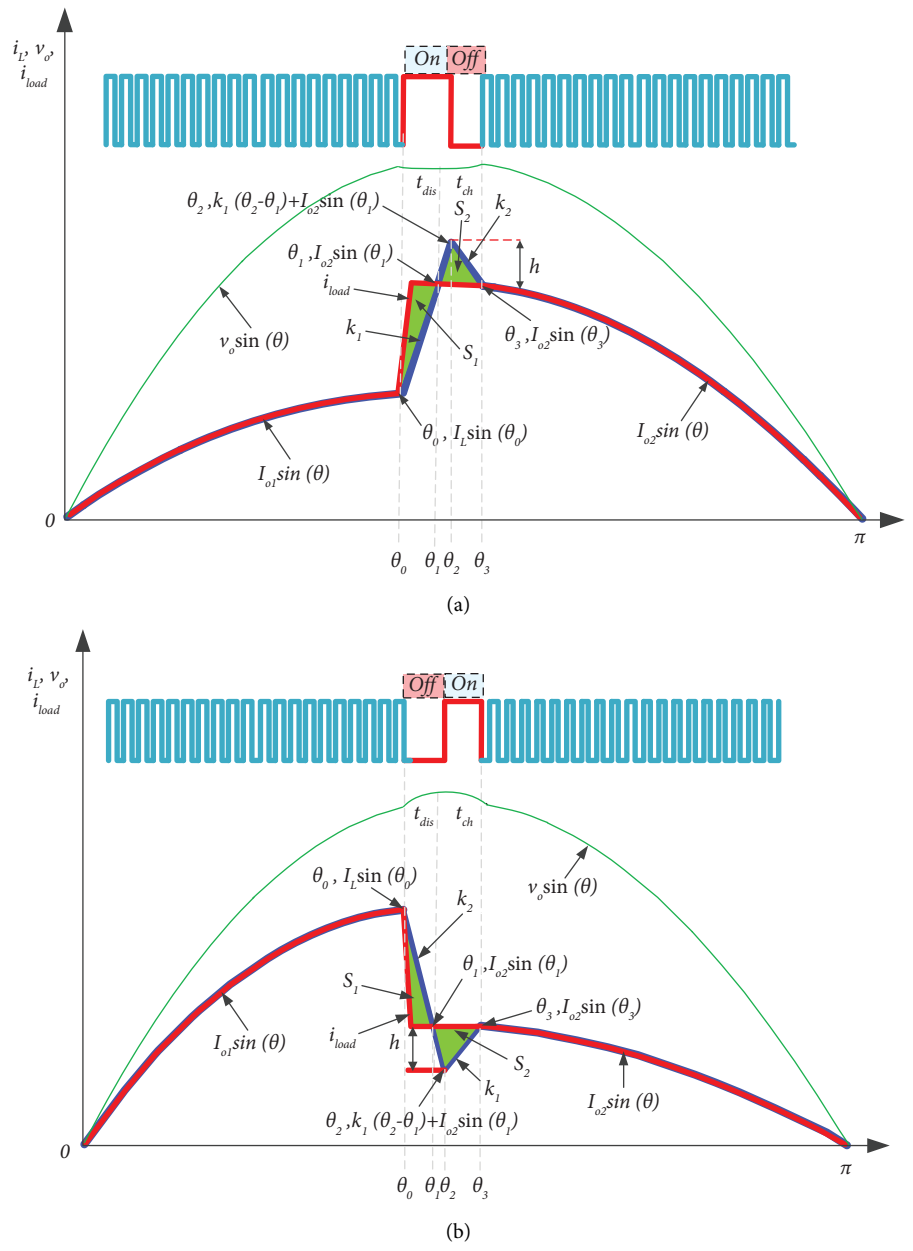

FIGURE 4: The transient response waveform with the optimal trajectory controller in response to load changes. (a) Positive step change. (b) Negative step change.

through (θ_2 and θ_3) is derived in (2) using the equivalent circuit depicted in Figure 2(b).

$$k_2 = \frac{-v_{in} - v_o \sin(\theta)}{2L\pi f_{line}}. \quad (2)$$

In the same way, the analysis described above can also be performed for single-phase VSIs with the optimal trajectory controller in response to a negative step change, as shown in Figure 4(b) which is as follows:

As seen in Figure 4, the proposed controller ensures that iL and vCf arrive at the desired value by precisely following the projected best trajectory while simultaneously reducing the settling time and voltage fluctuations that occur throughout the transient operation. Figure 5 indicates the operation diagram of the proposed predictive control algorithm in conjunction with the linear regulator. A digital control chip makes it easier to combine linear and nonlinear control algorithms to generate the PWM signal. All the transient switching state sequence and ON/OFF state time duration under the different load change conditions are calculated using on-line calculation or prestored off-line results as a look-up table in the on-chip flash. Furthermore, the linear controller parameters can be efficiently designed with relatively high bandwidth to handle the slow load change condition. Once the abrupt change in load current is noticed, the nonlinear controller quickly bypasses the linear regulator and controls the power devices in one switching period.

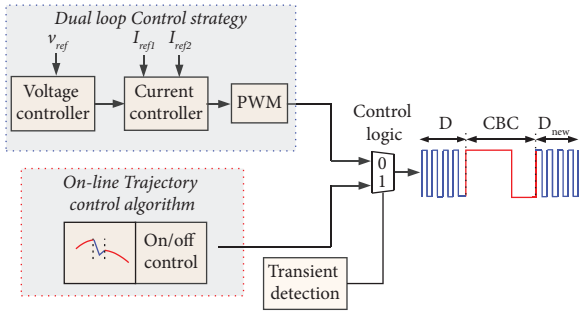

FIGURE 5: The on-line trajectory control algorithm in combination with the linear compensator.

4. Mathematical Derivation and Controller Design

The optimal trajectory control technique is implemented in four steps based on comprehensive theoretical research and mathematical derivation.

Step 1. Detection of load current step change at θ_0.

After detecting an abrupt change in load current, the on-line trajectory control module halts the linear controller. The power devices are instantly switched. $S_{ap} = S_{bn} = \text{ON}$ and $S_{an} = S_{bp} = \text{OFF}$ are fixed for step up, and $S_{an} = S_{bp} = \text{ON}$ and $S_{ap} = S_{bn} = \text{OFF}$ are fixed for step down.

Step 2. Calculate θ_1 and capacitor discharge portion S_1.

As shown in Figure 4(a), i_L goes up from $I_{o1}\sin(\theta_0)$ to $I_{o2}\sin(\theta_1)$, and C_f discharges between θ_0 and θ_1.

As demonstrated in Figure 4(a), i_L is rising from $I_{o1}\sin(\theta_0)$ to $I_{o2}\sin(\theta_1)$, and C_f is discharging during θ_0 and θ_1. Based on the current increasing slope coefficient k_1 expressed in (1), i_L meets

$$(I_{o2}\sin\theta_1 - I_{o1}\sin\theta_0) = k_1(\theta_1 - \theta_0). \tag{3}$$

The red waveform in Figure 4(a) shows that the load current does not significantly alter after the rapid step shift between θ_0 and θ_1, so $I_{o2}\sin\theta_1 \approx I_{o2}\sin\theta_0$. Equation (3) can be simplified, and θ_1 is calculated as follows:

$$\theta_1 = \frac{I_{o2}\sin\theta_0 - I_{o1}\sin\theta_0 + k_1\theta_0}{k_1}. \tag{4}$$

The green-shaded region S_1, representing the charge discharged by C_f, may be estimated using elementary geometric theory.

$$S_1 = \frac{1}{2}(\theta_1 - \theta_0)(I_{o2}\sin\theta_1 - I_{o1}\sin\theta_0) = \frac{1}{2}k_1(\theta_1 - \theta_0)^2. \tag{5}$$

Step 3. Calculate θ_2, θ_3, and capacitor charging portion S_2.

At θ_2, as presented in Figure 4(a), $S_{ap} = S_{bn} = \text{OFF}$ and $S_{an} = S_{bp} = \text{ON}$ are set. i_L begins to decline at the slope of k_2, and C_f starts to increase till θ_3. Throughout the transient θ_0 and θ_3, i_L encounters

$$I_{o1}\sin\theta_0 + k_1(\theta_2 - \theta_0) + k_2(\theta_3 - \theta_2) = I_{o2}\sin\theta_3. \tag{6}$$

Based on the green-shaded portion S_2, the charge absorbed by C_f can be calculated as follows:

$$S_2 = \frac{1}{2}(\theta_3 - \theta_1)(k_1(\theta_2 - \theta_1) + I_{o2}\sin\theta_1 - I_{o2}\sin\theta_3). \tag{7}$$

To ensure that both i_L and v_{cf} approach the region of the new quasi-steady state, the C_f released charge, represented by the green-shaded area S_1 during θ_0 and θ_1, should be equal to the absorbed charge, represented by S_2 during θ_1 and θ_3 and $S_1 = S_2$ as follows:

$$\begin{aligned}&(\theta_1 - \theta_0)(I_{o2}\sin\theta_1 - I_{o1}\sin\theta_0)\\ &\quad = (\theta_3 - \theta_1)(k_1(\theta_2 - \theta_1) + I_{o2}\sin\theta_1 - I_{o2}\sin\theta_3).\end{aligned} \tag{8}$$

Apparently, equations (6) and (8) are nonlinear equations that include two unknown variables, θ_2 and θ_3. It is easy to get the numerical solution of θ_2 and θ_3 using computer-assisted software such as Matlab or Mathcad.

Even though the accurate time instants θ_2 and θ_3 can be obtained using off-line numerical calculation, the on-line calculation is more suitable for practical engineering applications using a digital signal processor (DSP). Theoretical research and simulation demonstrate that the transient regulation time interval (θ_3–θ_0) is too short, so the load current can seem like a constant value. To simplify the calculation and apply the aforementioned optimal trajectory control algorithm in the C2000 DSP, some reasonable assumptions ($I_{o2}\sin\theta_3 \approx I_{o2}\sin\theta_2 \approx I_{o2}\sin\theta_1$) are made to simplify the analysis. Equations (6) and (8) are rewritten as follows:

$$\begin{cases} k_1(\theta_2 - \theta_0) + k_2(\theta_3 - \theta_2) \approx I_{o2}\sin\theta_0 - I_{o1}sin\theta_0, \\ (\theta_1 - \theta_0)^2 = (\theta_3 - \theta_1)(\theta_2 - \theta_1). \end{cases} \tag{9}$$

By solving (9), θ_2 and θ_3 are as follows:

$$\begin{cases} \theta_2 = \dfrac{2Xa + 2ak_1\theta_0 - k_2\left(-b \pm \sqrt{b^2 - 4ac}\right)}{2a(k_1 - k_2)}, \\ \theta_3 = \dfrac{-b \pm \sqrt{b^2 - 4ac}}{2a}, \end{cases} \tag{10}$$

in which $a = -k_2/k_1 - k_2$, $b = 1/k_1 - k_2(X - k_1\theta_1 + k_1\theta_0 + 2k_2\theta_1)$, $c = -X\theta_1 + k_1\theta_0\theta_1/k_1 - k_2 - \theta_0^2 + 2\theta_0\theta_1$, and $X = I_{o2}\sin\theta_0 - I_{o1}\sin\theta_0$.

Step 4. Trajectory control module deactivation (θ_3)

When i_L and v_{cf} enter the vicinity of a new quasi-steady state at θ_3, the trajectory control module is deactivated.

The entire settling period $\theta_{settling}$ for positive/negative step change described as θ_3–θ_0 is derived in (11).

$$\theta_{settling} = \frac{-b \pm \sqrt{b^2 - 4ac}}{2a} - \theta_0. \tag{11}$$

The suggested on-line optimal trajectory control approach equations were found for a step-up change in load

Table 1: The theoretical value and simplified calculation results for different step changes.

Operation conditions: $V_{\text{in}} = 200\,\text{V}$, $M = 0.78$, $L_f = 1.2\,\text{mH}$, $C_f = 20\,\mu\text{F}$, and $I_{o1} = 5\,\text{A}$					
Radians	20% step-up change	40% step-up change	60% step-up change	80% step-up change	100% step-up change
Positive step change at $\theta_0 = \pi/3$ (*theoretical value*)					
θ_{1t}	1.0522	1.0572	1.0622	1.0670	1.0724
θ_{2t}	1.0568	1.0664	1.0762	1.0856	1.0958
θ_{3t}	1.0577	1.0682	1.0789	1.0892	1.1004
Positive step change $\theta_0 = \pi/3$ (*simplified analytical solution*)					
θ_{1s}	1.0521	1.0570	1.0619	1.0668	1.0717
θ_{2s}	1.0566	1.0659	1.0753	1.0847	1.0941
θ_{3s}	1.0575	1.0677	1.0780	1.0883	1.0985
Positive step change at $\theta_0 = 2\pi/3$ (*theoretical value*)					
θ_{1t}	2.0992	2.1040	2.1088	2.1137	2.1182
θ_{2t}	2.1036	2.1127	2.1217	2.1310	2.1395
θ_{3t}	2.1044	2.1144	2.1243	2.1346	2.1439
Positive step change at $\theta_0 = 2\pi/3$ (*simplified analytical solution*)					
θ_{1s}	2.0993	2.1042	2.1091	2.1140	2.1189
θ_{2s}	2.1038	2.1131	2.1225	2.1319	2.1413
θ_{3s}	2.1047	2.1149	2.1252	2.1355	2.1457

current. The operating principles and equations for adapting the approach to a negative load current step change are almost identical to those described above.

Table 1 lists the theoretical value of θ_1, θ_2, and θ_3 by the numerical calculation and the analytical solution from the simplified equations (4) and (10) under the different load current step-change amplitude at $\pi/3$ and $2\pi/3$. The corresponding simplification error δ, defined as (12), is shown in Figure 6.

$$\delta = \frac{\theta_{3s} - \theta_0}{\theta_{3t} - \theta_0} \cdot 100\%. \tag{12}$$

The regulation time intervals of theoretical and simplified calculation results are approximately equivalent to each other, enabling the real-time on-line application and preserving enough control precision. δ grows as the step-change amplitude and filter inductance L increase. However, the slight simplification difference does not significantly impact the control performance.

The settling time of the on-line trajectory control algorithm during step change of load current is independent of the linear regulator parameters and mainly determined by the increasing and decreasing slopes of i_L, step-change initial angle θ_0, and amplitude. This is different from the dynamic behaviour of the single-phase VSI with the conventional controller because it does not use the output voltage as a feedback mechanism during the transient response from θ_0 to θ_3.

Figure 7 shows the program flow chart of the on-line trajectory control algorithm. After detecting the rapid step change, the transient regulation module is activated. In the end, the control system returns to using the linear regulator. Figure 8 illustrates the total settling time for the single-phase VSI with different inductance L_f, θ_0, and amplitude under the operation conditions $v_{in} = 200\,\text{V}$, $v_o = 154\,\text{V}$, and $I_{o1} = 5\,\text{A}$.

From the previous analysis, the on-line trajectory control algorithm is more suitable for the dramatic load change. It does not work well under relatively small or slow load change conditions in the vicinity of 0 and π, as shown in Figure 9. A linear regulator can work very well in these operating conditions and provide a good dynamic performance.

5. Implementation Techniques for the Detection of Critical Points for Transferring

The proposed implementation techniques that can be used to detect these critical points and provide a seamless transition between controllers are given as follows:

5.1. Detection of Load Step Changes. The proposed load step detection approach uses analog and digital signal processing techniques. A delayed output voltage signal and a comparator are used to detect load step changes in a power supply or load. The delayed signal is generated by a simple RC filter circuit, and the comparator generates a pulse signal if their difference exceeds a certain threshold. The microcontroller processes the comparison results to realize the step detection of load. Figure 10 shows a load change detector circuit with an adjustable delay.

5.2. Smooth Transferring Back to Linear Control. To transition smoothly to the linear controller, this article suggests increasing sampling frequency, maximizing system bandwidth, and running the linear controller at max speed. After the transient, the control system reverts to the PI controller for steady-state regulation. Before reverting to the linear controller, the optimal approach computes new steady-state values denoted as $i_{L\text{new}}$ and D_{rew} for inductor current and duty cycle to avoid oscillations.

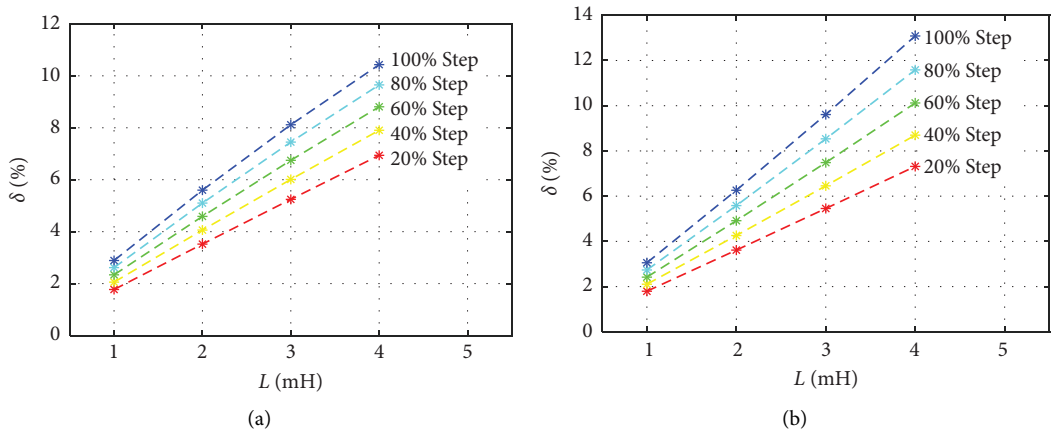

Figure 6: The simplification error δ under different inductance and load current step change at $V_{in} = 200$ V, $v_o = 154$ V, and $I_{o1} = 5$ A: (a) positive step change ($\theta_0 = \pi/3$) and (b) positive step-change ($\theta_0 = 2\pi/3°$).

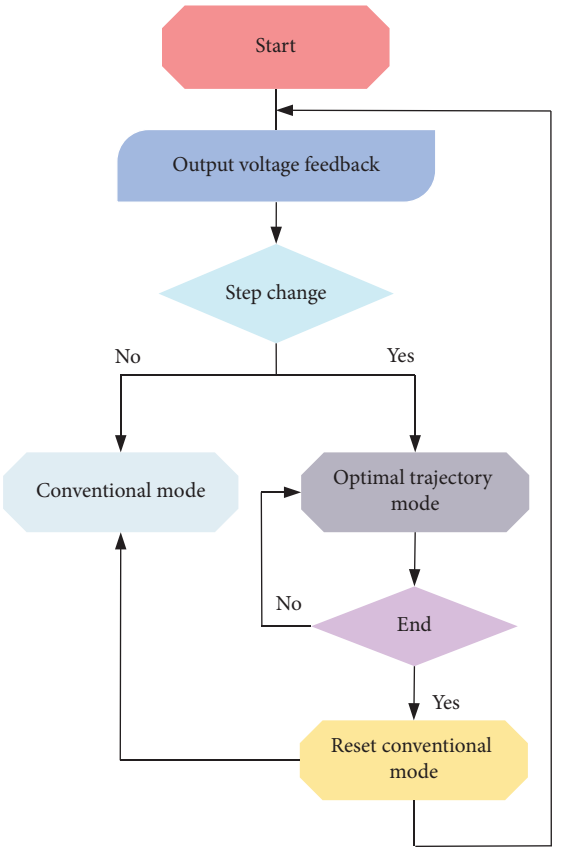

Figure 7: Flow chart of the on-line optimal trajectory control algorithm under the different load step change.

$$i_{L\text{new}} = I_{o2} \sin(\theta_3),$$
$$D_{\text{new}} = \frac{1 + M_i \sin(\theta_3)}{2}. \quad (13)$$

6. Simulation and Experiment Results

Numerical simulations in MATLAB/Simulink were used to evaluate the suggested on-line trajectory control approach and theoretical analysis. For comparison, a well-designed

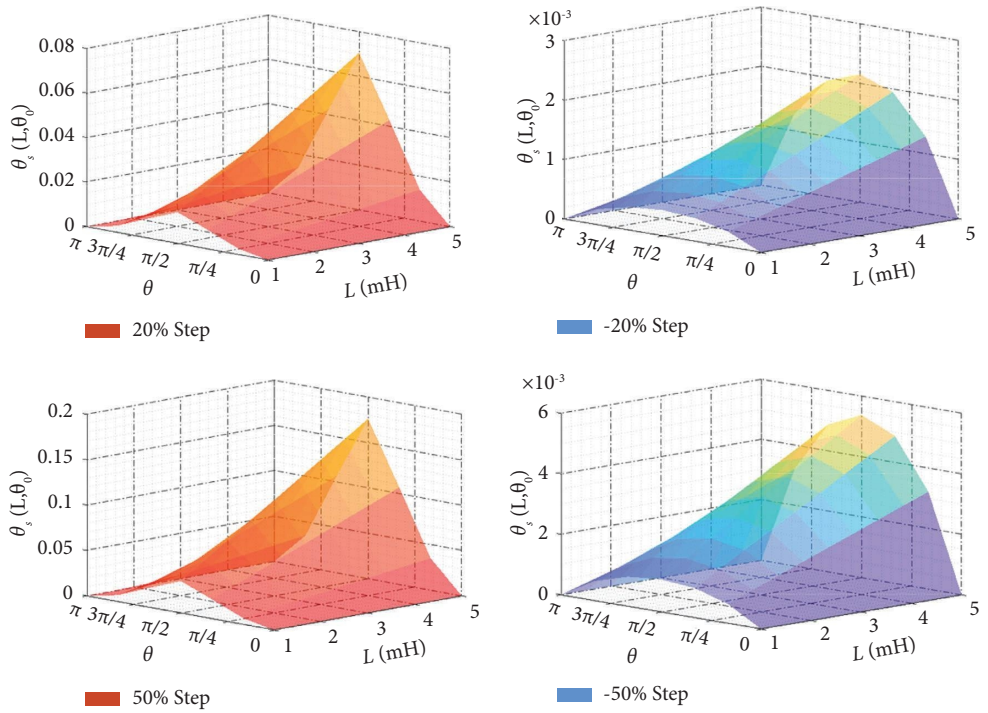

Figure 8: The settling time with the on-line trajectory controller under different inductance and load current step change.

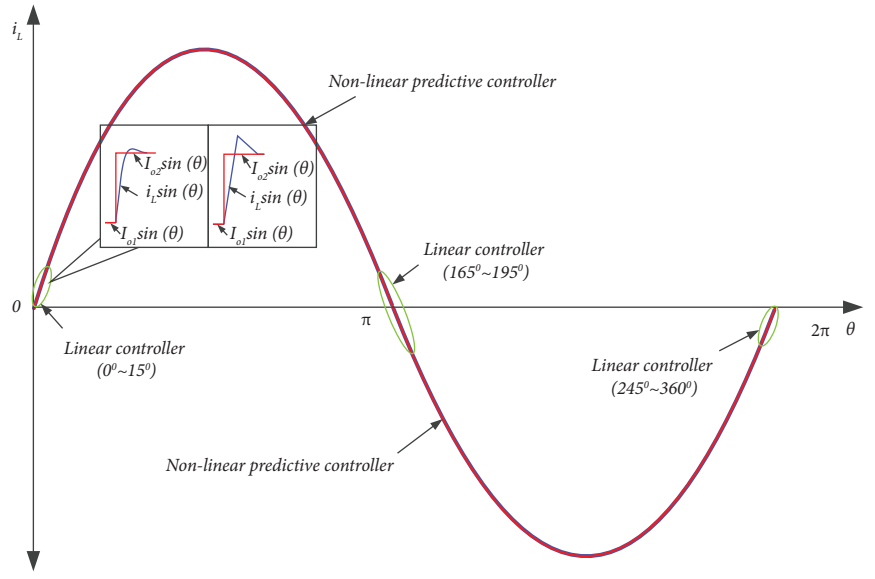

Figure 9: The suitable load step-change condition for the single-phase VSI with the on-line trajectory control algorithm.

single-phase VSI with a linear controller is constructed. The main circuit parameters are $v_{in} = 200$ V, $v_o = 154$ V, $C_1 = C_2 = 5000$ uF, $L_f = 1$ mH, $C_f = 20$ uF, $R_{L1} = 20\,\Omega$, and $R_{L2} = 50\,\Omega$. The switching frequency f_s is 100 kHz, and the output line frequency f_{line} is 50 Hz. The main parameters of the PI controller are $k_{vol}(z) = 0.5 + 0.005\ z/(z-1)$ and $k_{\text{cur}}(z) = 4.2 + 0.025\ z/(z-1)$.

The transient response of DC-AC with a traditional PI controller to load current ranging from 7.8 A to 10.5 A and back to 7.8 A is presented in Figure 11, and Figure 12 depicts the transient response utilizing the on-line trajectory method. The measured waveforms comprise the identified load step-change signals, V_{ab}, i_L, and v_{Cf}.

To control i_L and v_C from the one steady state $i_{L\_\text{int}} = 7.8$ A and $v_{cf\_\text{int}} = 133.36$ V to the final steady state $i_{L\_\text{final}} = 10.5$ A and $v_{cf\_final} = 136.36$ V, the optimal trajectory of a transient is predicted and implemented. According to (4) and (10), the on-state time interval of S_a 116 μs and off-state time interval 10 μs calculated in the theory for positive step change are identical to the

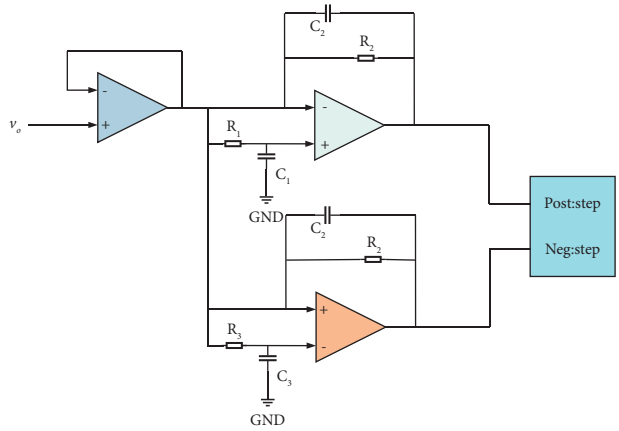

Figure 10: Implementation of the load change detector.

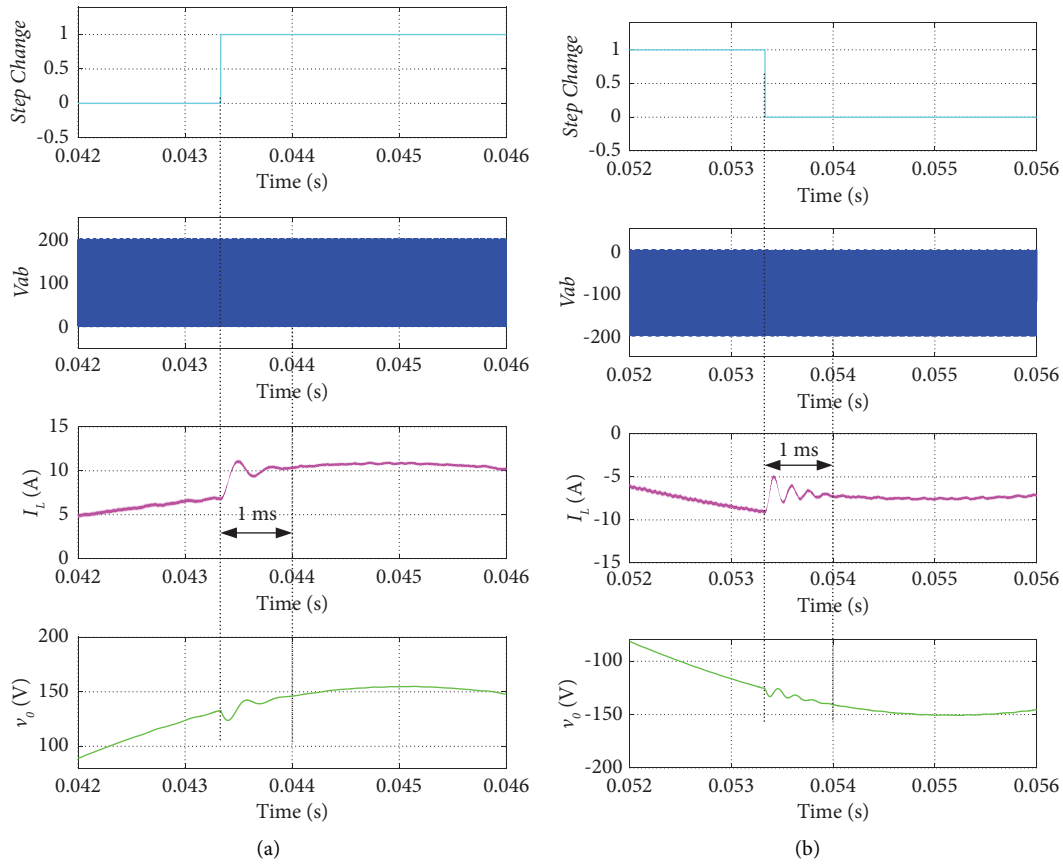

Figure 11: Transient response load current with linear control. (a) Step up from 7.8 A to 10.5 A at $\pi/3$. (b) Step down from 10.5 A to 7.8 A at $4\pi/3$.

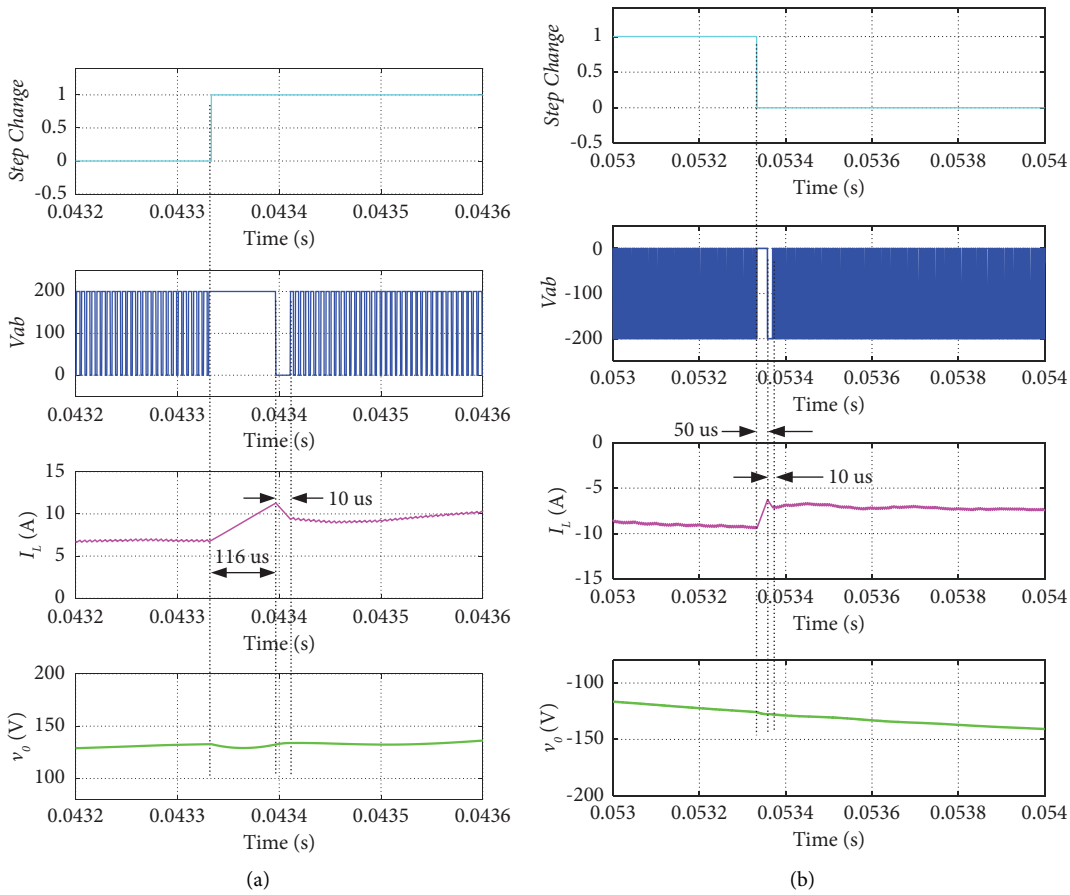

Figure 12: Transient response with on-line trajectory control. (a) Step up from 7.8 A to 10.5 A at $\pi/3$. (b) Step-down from 10.5 A to 7.8 at $4\pi/3$.

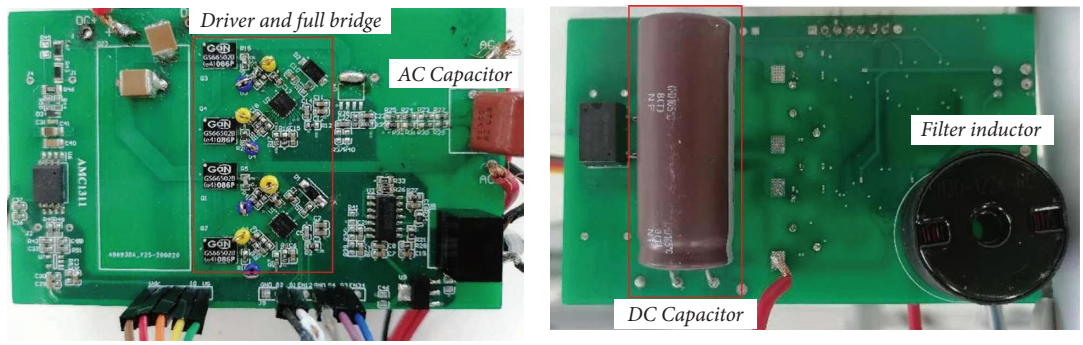

Figure 13: The prototype of the single-phase VSI. (a) Top view. (b) Bottom view.

simulation results displayed in Figure 12(a). The recovery period is decreased from 1 ms to 126 μs, which is a more than 80% decrease compared to a traditional dual-loop linear PI controller. Additionally, voltage undershoot is significantly decreased.

It is demonstrated in Figure 12(b) that with load current ranging from 10.5 A to 7.7 A, the transient settling time is reduced from 1 ms with the conventional dual-loop controller to 60 us using the on-line trajectory control algorithm.

As illustrated in Figure 13, a laboratory prototype of the 800 W single-phase VSI is constructed to validate the theoretical calculations, and the corresponding system diagram is shown in Figure 14. The six-step on-line trajectory control method can be readily created and executed using the EPWM and high-speed ADC capabilities of the TMS320F28377D. Each switching instant's duration is computed on-line and saved on a chip. AC load step change is executed via a bidirectional switch with two MOSFETs linked in reverse. In addition, the

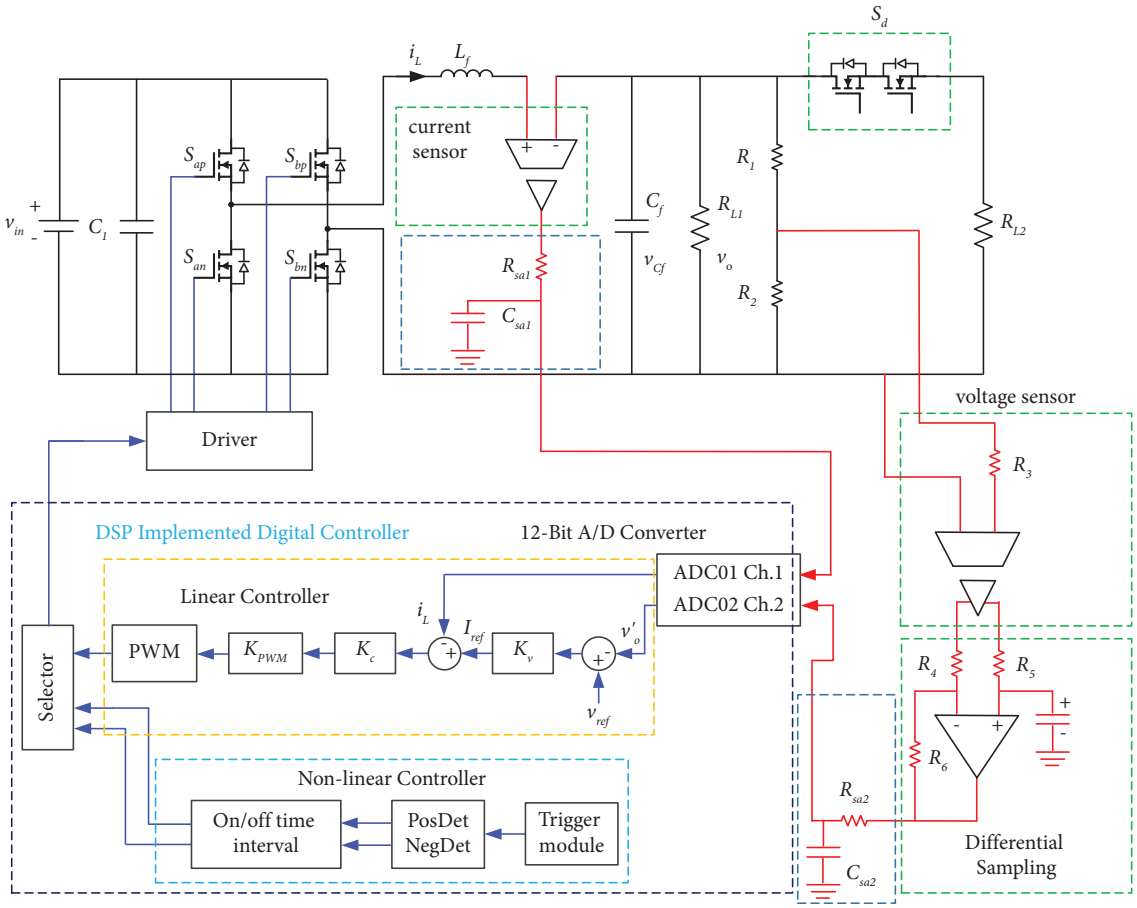

Figure 14: The hardware implementation block diagram of the proposed controller.

Table 2: The specifications for the experimental prototype.

Switching device	S_{ap}, S_{an}, S_{bp}, S_{bn} S_d	GAN (GS65004B) MOSFET (SiHJ6N65E)
Passive components	C_{dc} L_f C_f	5000 uF 0.5 mH 20 μF
R_L load	R_{L1} R_{L2}	30 Ω 50 Ω
Switching frequency	f_s	100 kHz
Current sensor Voltage sensor	K_i K_v	0.1 0.01

external interrupt is employed to identify the abrupt change in load current i_L, and v_{cf} is measured using two operational amplifiers with excellent bandwidth and isolation. The voltage and current loop's PI controller guarantees that v_o tracks the reference with zero steady-state error. The PWM module then creates four driving signals for power devices. As soon as a step-change is recognized, the linear controller shifts to a nonlinear optimal controller.

The on/off time module generates a control signal according to the calculated time instants. PI parameters are reset at the completion of the transient, and the control system is switched back to the linear regulator. The controller undergoes a smooth transition with negligible switchover effects because v_o, i_L, and Dnew are at their new quasi-steady-state values. A "slow" PI controller does not need to maintain stability during mode switchovers. Consequently, the maximum speed of the linear control may be attained. Table 2 lists the specifications of the experimental prototype, and key parameters of dual-loop PI controllers are $k_{vol}(z) = 0.2 + 0.0034 \cdot z/(z-1)$ and $k_{cur}(z) = 1.2 + 0.017\, z/(z-1)$. Two step-change points, $\pi/3$ and $4\pi/3$, are chosen for the hardware demonstration of the on-line trajectory control algorithm. Figure 15 illustrates the transient

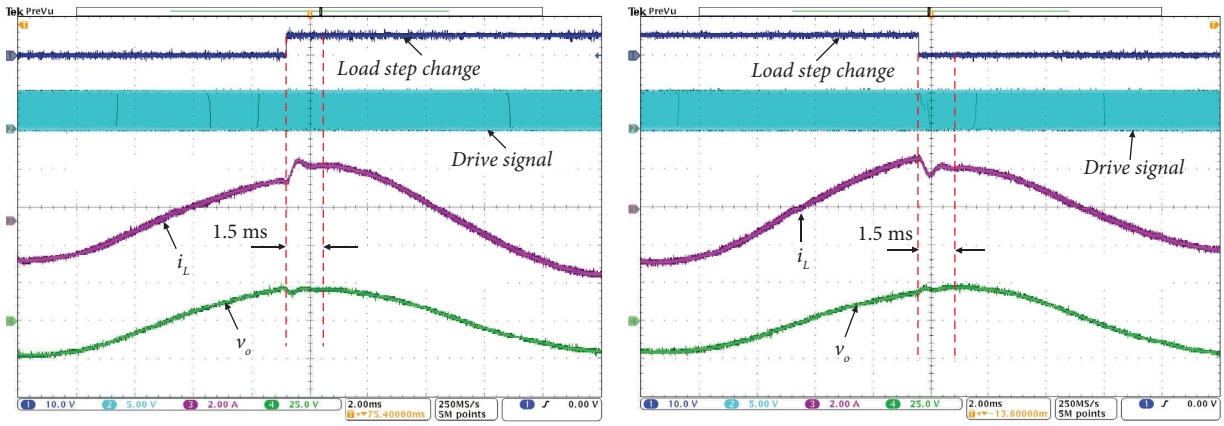

(a) (b)

Figure 15: Transient waveforms with the PI controller at $\pi/3$. (a) Step change of i_{load} from 2.2 A to 3.5 A. (b) Step change of i_{load} from 3.5 A to 2.2 A.

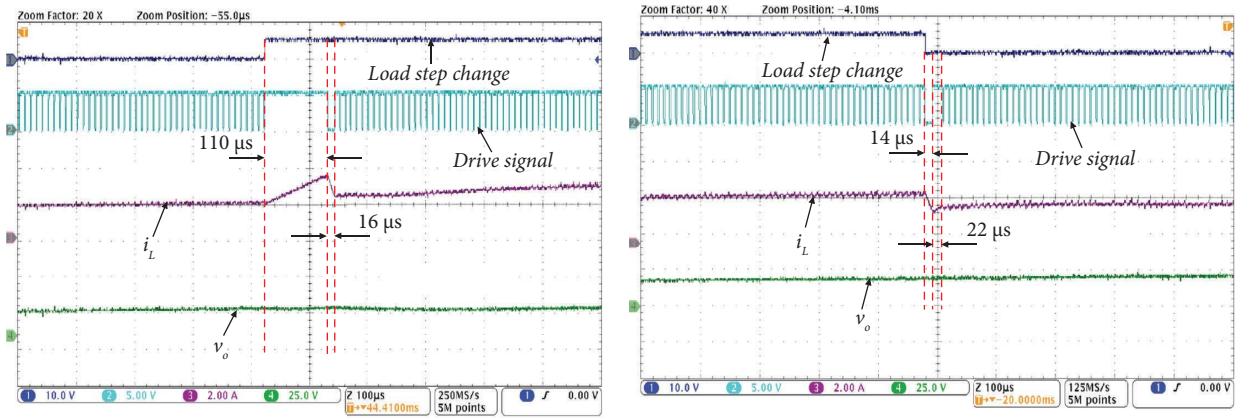

(a) (b)

Figure 16: Transient waveforms of the proposed controller at $\pi/3$. (a) Step change of i_{load} from 2.2 A to 3.5 A. (b) Step change of i_{load} from 3.5 A to 2.2 A.

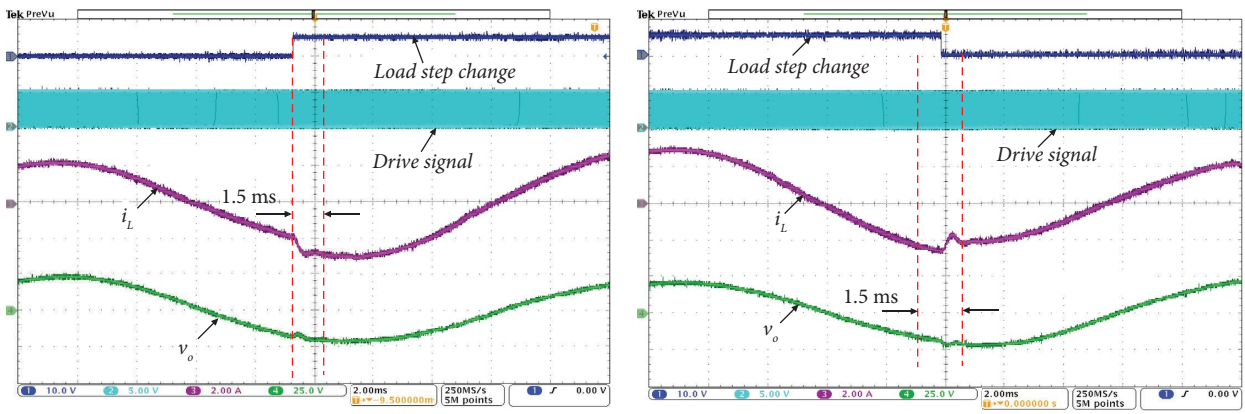

(a) (b)

Figure 17: Transient waveforms with the PI controller at $4\pi/3$. (a) Step change of i_{load} from 2.2 A to 3.5 A. (b) Step change of i_{load} from 3.5 A to 2.2 A.

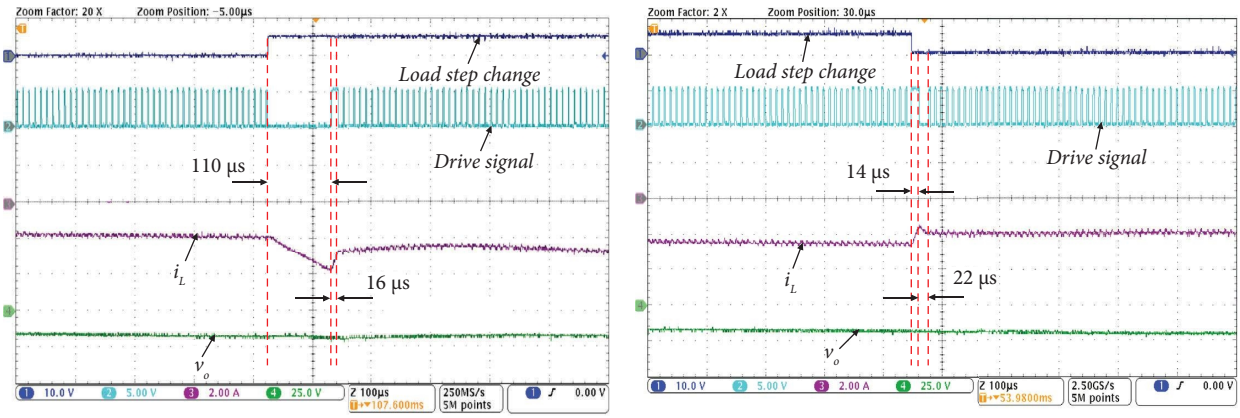

(a) (b)

FIGURE 18: Transient waveforms of the proposed controller at $4\pi/3$. (a) Step change of i_{load} from 2.2 A to 3.5 A. (b) Step change of i_{load} from 3.5 A to 2.2 A.

experimental waveforms of a single-phase VSI with the linear controller during a rapid step change at $\pi/3$. And Figure 16 depicts the similar transient response of the suggested nonlinear optimal trajectory control approach during the identical step change in load current. Both v_{Cf} and i_L recover rapidly. The settling time using the on-line trajectory control method is approximately consistent with the theoretical calculation, coming in at 113 microseconds for positive step changes in load current and 36 microseconds for negative step changes in load current.

The voltage/current overshoot and oscillation amplitude throughout the transient process are smaller than the simulation value due to the hardware test platform's relatively large system damping coefficient. Figures 17 and 18 show the measured experimental results of the single-phase VSI with the existing linear controller and the on-line trajectory control algorithm during step change at $4\pi/3$, respectively.

7. Conclusion

This article presents a hardware-efficient, low cost, and simple on-line trajectory controller with the following merits: The controller can work conveniently (bandwidth-free) with a linear-nonlinear combination without sacrificing stability or having any steady-state errors. The controller is far superior to conventional methods, in addition to being less complicated, less expensive, and having fewer limitations than the control methods mentioned above. The voltage deviation may be lowered by 74%, and the settling time can be reduced by 80% in response to the load current step change in a positive direction. On the other hand, if the load current is altered in a negative direction, the converter overshoot will be reduced by 70%, and the settling time will be cut down by 75%. At the same time, a set of nonlinear optimization equations are constructed, which can change the output voltage according to the application scene and realize the real-time on-line control. Simulation and experimental platforms are built to verify the proposed scheme's correctness. The results show that the proposed control scheme can effectively shorten the stabilization time, reduce the voltage spike in the transient state process, and improve the reliability of the equipment.

Nomenclature

K_1: Upward slope
K_2: Downward slope
S_1: Charge portion
S_2: Discharge portion of
i_L: Inductor current
i_{load}: Load current
i_{ref}: Reference current
i_L: Sensed current
v_{ref}: Reference voltage
I_{o1}: Initial load current
I_{o2}: Final load current
v_{in}: Input dc voltage
v_o: Output voltage
v_{cf}: Capacitor voltage
L_f: Filter inductor
C_f: Filter capacitor
S_d: SSR relay switch
R_{L1}: Initial load
R_{L2}: Second load
D_{new}: New duty ratio
f_{line}: Line frequency.

Data Availability

No data were used to support this study.

Conflicts of Interest

The authors declare that they have no conflicts of interest.

Acknowledgments

The study was supported by University Enterprise Fund.

References

[1] J.-M. Park, K.-H. Lee, Y.-J. Park, J.-H. Lee, and C.-Y. Won, "Predictive control for single-phase multi-module UPS inverters with output LC filter modeling," in *Proceedings of the 2017 20th International Conference on Electrical Machines and Systems (ICEMS)*, pp. 1–6, Sydney, NSW, Australia, August 2017.

[2] H. Komurcugil, "Improved passivity-based control method and its robustness analysis for single-phase uninterruptible power supply inverters," *IET Power Electronics*, vol. 8, no. 8, pp. 1558–1570, 2015.

[3] P. Nithara and R. P. Eldho, "Comparative analysis of different control strategies in single phase standalone inverter," in *Proceedings of the 2021 7th International Conference on Advanced Computing and Communication Systems (ICACCS)*, pp. 1105–1109, Coimbatore, India, March 2021.

[4] X. Wang, X. Zhou, and H. Wang, "Optimizing PI controller of the single-phase inverter based on FOA," in *Proceedings of the 2017 2nd International Conference on Robotics and Automation Engineering (ICRAE)*, pp. 151–155, Shanghai, China, December 2017.

[5] R. Errouissi, H. Shareef, and A. Wahyudie, "A novel design of PR controller with antiwindup scheme for single-phase interconnected PV systems," *IEEE Transactions on Industry Applications*, vol. 57, no. 5, pp. 5461–5475, 2021.

[6] S. Essaghir, M. Benchagra, and N. El barbri, "Comparison between PI and PR current controllers of a grid- connected photovoltaic system under load variation," *International Journal of Power Electronics and Drive Systems*, vol. 9, no. 3, p. 1311, 2018.

[7] M. Parvez, M. F. M. Elias, and N. A. Rahim, "Performance analysis of PR current controller for single-phase inverters," in *Proceedings of the 4th IET Clean Energy and Technology Conference (CEAT 2016)*, pp. 1–8, Kuala Lumpur, Malaysia, November 2016.

[8] S. Kuroda, K. Natori, and Y. Sato, "PI current control method for realizing deadbeat characteristics," in *Proceedings of the 2022 International Power Electronics Conference (IPEC-Himeji 2022- ECCE Asia)*, pp. 57–62, Himeji, Japan, May 2022.

[9] R. Gupta, "Generalized frequency domain formulation of the switching frequency for hysteresis current controlled VSI used for load compensation," *IEEE Transactions on Power Electronics*, vol. 27, no. 5, pp. 2526–2535, 2012.

[10] Z. Yao and L. Xiao, "Two-switch dual-buck grid-connected inverter with hysteresis current control," *IEEE Transactions on Power Electronics*, vol. 27, no. 7, pp. 3310–3318, 2012.

[11] H. Mao, X. Yang, Z. Chen, and Z. Wang, "A Hysteresis current controller for single-phase three-level voltage source inverters," *IEEE Transactions on Power Electronics*, vol. 27, no. 7, pp. 3330–3339, 2012.

[12] L. Zhang, R. Born, B. Gu et al., "A sensorless implementation of the parabolic current control for single-phase stand-alone inverters," *IEEE Transactions on Power Electronics*, vol. 31, no. 5, pp. 3913–3921, 2016.

[13] G. Wang and Y. W. Li, "Parabolic PWM for current control of voltagesource converters (VSCs)," *IEEE Transactions on Industrial Electronics*, vol. 57, no. 10, pp. 3491–3496, 2010.

[14] A. Abrishamifar, A. A. Ahmad, and M. Mohamadian, "Fixed switching frequency sliding mode control for single-phase unipolar inverters," *IEEE Transactions on Power Electronics*, vol. 27, no. 5, pp. 2507–2514, 2012.

[15] H. Komurcugil, "Rotating-sliding-line-basedsliding-mode control for single-phase UPS inverters," *IEEE Transactions On Industrial Electronics*, vol. 59, no. 10, pp. 3719–3726, 2012.

[16] T.-L. Tai and J.-S. Chen, "UPS inverter design using discrete-time sliding-mode control scheme," *IEEE Transactions on Industrial Electronics*, vol. 49, no. 1, pp. 67–75, 2002.

[17] K. Au, C. Ho, H. Chung, W. H. Lau, and W. T. Yan, "Digital implementation of boundary control with second-order switching surface for inverters," in *Proceedings of the 2007 IEEE Power Electronics Specialists Conference*, pp. 1658–1664, Orlando, FL, USA, June 2007.

[18] W. T. Yan, C. Ho, H. Chung, and K. Au, "Fixed-frequency boundary control of buck converter with second-order switching surface," *IEEE Transactions on Power Electronics*, vol. 24, no. 9, pp. 2193–2201, Sept. 2009.

[19] M. Pokharel, N. Hildebrandt, C. N. M. Ho, and Y. He, "A fast-dynamic unipolar switching control scheme for single-phase inverters in DC microgrids," *IEEE Transactions on Power Electronics*, vol. 34, no. 1, pp. 916–927, Jan. 2019.

[20] S. P. Ribas, L. A. Maccari Jr., H. Pinheiro, R. C. D. L. F. Oliveira, and V. F. Montagner, "Design and implementation of a discrete-time H-infinity controller for uninterruptible power supply systems," *IET Power Electronics*, vol. 7, no. 9, pp. 2233–2241, 2014.

[21] A. Soto, P. Alou, J. A. Oliver, J. A. Cobos, and J. Uceda, "Optimum control design of PWM-buck topologies to minimize output impedance," in *Proceedings of the APEC. Seventeenth Annual IEEE Applied Power Electronics Conference and Exposition (Cat. No.02CH37335)*, pp. 426–432, Dallas, TX, USA, March 2002.

[22] A. Kelly and K. Rinne, "Sensorless current-mode control of a digital dead-beat DC-DC converter," in *Proceedings of the Nineteenth Annual IEEE Applied Power Electronics Conference and Exposition, 2004. APEC' 04*, vol. 3, pp. 1790–1795, Anaheim, CA, USA, February 2004.

[23] K. S. Leung and H. S. Chung, "Dynamic hysteresis band control of the buck converter with fast transient response," *IEEE Transactions on Circuits and Systems II: Express Briefs*, vol. 52, no. 7, pp. 398–402, 2005.

[24] K. S. Leung and H. S. Chung, "Derivation of a second-order switching surface in the boundary control of buck converters," *IEEE Power Electronics Letters*, vol. 2, no. 2, pp. 63–67, June 2004.

[25] K. S. Leung and H. S. Chung, "A comparative study of the boundary control of buck converters using first- and second-order switching surfaces–Part I: continuous conduction mode," in *Proceedings of the 2005 IEEE 36th Power Electronics Specialists Conference*, pp. 2133–2139, Recife, Brazil, June 2005.

[26] K. S. Leung and H. S. Chung, "A comparative study of boundary control with first- and second-order switching surfaces for buck converters operating in DCM," *IEEE Transactions on Power Electronics*, vol. 22, no. 4, pp. 1196–1209, 2007.

[27] A. Soto, A. P. Alou, and J. A. Cobos, "Non-linear digital control breaks bandwidth limitations," in *Proceedings of the Twenty-First Annual IEEE Applied Power Electronics Conference and Exposition*, pp. 42–47, Dallas, TX, USA, March 2006.

[28] G. Feng, W. Eberle, and Y. Liu, "A new digital control algorithm to achieve optimal dynamic performance in DC-DC converters," *Proc. IEEE PESC Conf*, vol. 22, pp. 2744–2748, 2005.

[29] G. Feng, W. Eberle, and Y. Liu, "High performance digital control algorithms for DC-DC converters based on the principle of capacitor charge balance," in *Proceedings of the 2006 37th IEEE Power Electronics Specialists Conference 2006*, pp. 1740–1743, Jeju, Korea (South), Jun 2006.

[30] G. Feng, E. Meyer, and Y. F. Liu, "Novel digital controller improves dynamic response and simplifies design process of voltage regulator module," in *Proceedings of the APEC 07 - Twenty-Second Annual IEEE Applied Power Electronics Conference and Exposition*, pp. 1447–1453, Anaheim, CA, USA, February 2007.

[31] G. Feng, E. Meyer, and Y. F. Liu, "A new digital control algorithm to achieve optimal dynamic performance in DC-to-DC converters," *IEEE Transactions on Power Electronics*, vol. 22, no. 4, pp. 1489–1498, 2007.

[32] S. Zaman, Y. zhang, L. Jinjun, L. Xinying, N. Ali Larik, and Z. Jinshui, "Dynamic performance improvement of single-phase dc-ac converter with non-linear digital predictive control," in *Proceedings of the 2020 IEEE Energy Conversion Congress and Exposition (ECCE)*, pp. 5263–5268, Detroit, MI, USA, October 2020.